ISSN 1674-1056
http://cpb.iphy.ac.cn
http://iopscience.iop.org/cpb
中国物理 B
Chinese Physics
中国物理 Chinese Physics B

Novel hole transport layer of nickel oxide composite with carbon for high-performance perovskite solar cells

Sajid, Elseman A M, Jun Ji(纪军), Shangyi Dou(窦尚轶), Hao Huang(黄浩), Peng Cui(崔鹏), Dong Wei(卫东), Meicheng Li(李美成)
Citation: Chin. Phys. B . 2018, 27(1): 017305. **doi:** 10.1088/1674-1056/27/1/017305

Journal homepage: http://cpb.iphy.ac.cn; http://iopscience.iop.org/cpb

What follows is a list of articles you may be interested in

Effect of metal catalyst on the mechanism of hydrogen spillover in three-dimensional covalent-organic frameworks

Xiu-Ying Liu(刘秀英), Jing-Xin Yu(于景新), Xiao-Dong Li(李晓东), Gui-Cheng Liu(刘桂成), Xiao-Feng Li(李晓凤), Joong-Kee Lee
Chin. Phys. B . 2017, 26(2): 027302. **doi:** 10.1088/1674-1056/26/2/027302

Charge susceptibilities of armchair graphene nanoribbon in the presence of magnetic field

H Rezania, F Azizi
Chin. Phys. B . 2016, 25(9): 097303. **doi:** 10.1088/1674-1056/25/9/097303

Scaling dependence of memory windows and different carrier charging behaviors in Si nanocrystal nonvolatile memory devices

Jie Yu(于杰), Kun-ji Chen(陈坤基), Zhong-yuan Ma(马忠元), Xin-xin Zhang(张鑫鑫), Xiao-fan Jiang(江小帆), Yang-qing Wu(吴仰晴), Xin-fan Huang(黄信凡), Shunri Oda
Chin. Phys. B . 2016, 25(9): 097304. **doi:** 10.1088/1674-1056/25/9/097304

Structural, electronic, and magnetic properties of transition-metal atom adsorbed two-dimensional GaAs nanosheet

Jia Luo(罗佳), Gang Xiang(向钢), Tian Yu(余天), Mu Lan(兰木), Xi Zhang(张析)
Chin. Phys. B . 2016, 25(9): 097305. **doi:** 10.1088/1674-1056/25/9/097305

Theoretical study of molecular hydrogen and spiltover hydrogen storage on two-dimensional covalent-organic frameworks

Liu Xiu-Ying, He Jie, Yu Jing-Xin, Li Zheng-Xin, Fan Zhi-Qin
Chin. Phys. B . 2014, 23(6): 067303. **doi:** 10.1088/1674-1056/23/6/067303

SPECIAL TOPIC — New generation solar cells

Novel hole transport layer of nickel oxide composite with carbon for high-performance perovskite solar cells*

Sajid[1], A M Elseman[1,2], Jun Ji(纪军)[1], Shangyi Dou(窦尚轶)[1], Hao Huang(黄浩)[1], Peng Cui(崔鹏)[1], Dong Wei(卫东)[1], and Meicheng Li(李美成)[1,†]

[1] *State Key Laboratory of Alternate Electrical Power, System with Renewable Energy Sources, School of Renewable Energy, North China Electric Power University, Beijing* 102206, *China*

[2] *Electronic & Magnetic Materials Department, Advanced Materials Division, Central Metallurgical Research and Development Institute (CMRDI), Helwan, Cairo* 11421, *Egypt*

(Received 14 October 2017; revised manuscript received 18 October 2017; published online 21 December 2017)

A depth behavioral understanding for each layer in perovskite solar cells (PSCs) and their interfacial interactions as a whole has been emerged for further enhancement in power conversion efficiency (PCE). Herein, NiO@Carbon was not only simulated as a hole transport layer but also as a counter electrode at the same time in the planar heterojunction based PSCs with the program wxAMPS (analysis of microelectronic and photonic structures)-1D. Simulation results revealed a high dependence of PCE on the effect of band offset between hole transport material (HTM) and perovskite layers. Meanwhile, the valence band offset ($\Delta E_{\rm v}$) of NiO-HTM was optimized to be −0.1 to −0.3 eV lower than that of the perovskite layer. Additionally, a barrier cliff was identified to significantly influence the hole extraction at the HTM/absorber interface. Conversely, the $\Delta E_{\rm v}$ between the active material and NiO@Carbon-HTM was derived to be −0.15 to 0.15 eV with an enhanced efficiency from 15% to 16%.

Keywords: hole transporting materials, counter electrode, perovskite solar cells, simulation

PACS: 73.22.–f **DOI:** 10.1088/1674-1056/27/1/017305

1. Introduction

Metal halide perovskite solar cells (PSCs) have been emerged as a kind of encouraging alternatives to existing photovoltaic technologies with both solution-processability and superior photovoltaic performance. Fundamental studies on perovskite materials,[1] device designs,[2,3] fabrication processes,[4–6] and materials engineering[7–13] have boosted the rapid development of PSCs. Consequently, a certified power conversion efficiency (PCE) of 22.1% have been obtained after the past several years of vigorous work. However, despite the overwhelming achievements in terms of performance of PSCs and long-term stability, current-voltage hysteresis still remains critical.[4] In order to obtain such enhanced performance and better stability, different organic and inorganic p-type semiconductor materials have been incorporated as hole extraction/hole transport layers (HTLs) in PSCs.[14–19] Among these, inorganic p-type semiconductors are particularly attractive due to their high transmittance, high hole mobility, and high chemical stability.[14,15] Especially, nickel oxide (NiO) is an attractive inorganic p-type semiconductor since it can be readily deposited by a variety of methods. In addition, it has good chemical stability, excellent transmittance, wide band gap, and convenient energy level alignment with the perovskite. Collectively these properties facilitate hole collection and electron blocking.[20–39] Thus, the stability of PSCs based on NiO-HTL has been significantly improved compared to commonly used poly (3, 4-ethylene dioxythiophene): polystyrene sulfonate (PDOT:PSS).[40,41] However, the achieved PCEs of NiO-based PSCs still lag behind of those established PSCs.[42,43] The conductivity of NiO can be increased by adjusting the stoichiometry of the films or by doping, while the implementation as top HTL via solvent engineering. Stoichiometric NiO is insulating, while the commonly observed p-type conductivity in undoped NiO is typically attributed to the nickel vacancies.[44,45] However, the hole density in undoped NiO is limited due to the large ionization energy of Ni vacancies. The hole density can be increased by extrinsic dopants with more shallow acceptor levels.[45] Indeed, the low conductivity and deposition of NiO as top HTL need to be addressed.[43] The common dopant used for NiO is Li, although other dopants such as Cu,[46–48] Mg, Co, as well as co-doping approach with Li:Cu and Cs:Li[42,49,50] have been reported. The doped NiO HTLs such as Cu:NiO_x,[46] LiCu:NiO_x,[50] MgLi:NiO_x,[41] and Cs:NiO_x[42] have displayed PCEs of 17.30%, 14.53%,

*Project supported by the National High-tech Research and Development Program of China (Grant No. 2015AA034601), the National Natural Science Foundation of China (Grant Nos. 51772096, 91333122, 51372082, 51402106, and 11504107), the Ph.D. Programs Foundation of Ministry of Education of China (Grant No. 20130036110012), the Par-Eu Scholars Program, Beijing Municipal Science and Technology Project, China (Grant No. Z161100002616039), and the Fundamental Research Funds for the Central Universities of China (Grant Nos. 2016JQ01, 2015ZZD03, 2015ZD07, and 2017ZZD02).

†Corresponding author. E-mail: mcli@ncepu.edu.cn

© 2018 Chinese Physical Society and IOP Publishing Ltd

18.3% and 19.35%, respectively. However, NiO@carbon composite is not applied to photovoltaic devices so far. Therefore, the incorporation of NiO@carbon-HTM with high conductivity and counter electrode behavior could be an effective way to achieve highly efficient PSCs at low cost. In simulation, the valence band offset (ΔE_v) of NiO-HTM was calculated to be -0.1 to 0.3 eV with high barrier cliff for the hole extraction at the HTM/perovskite interface. Conversely, ΔE_v between perovskite and NiO@carbon-HTM was derived to be -0.15 to 0.15 eV with an enhanced efficiency from 15% to 16%.

Herein, our work focused on the design of high-efficiency PSCs through investigating NiO@carbon material as top HTL with counter electrode characteristics. The comparison between NiO and NiO@carbon was simulated based on PSCs with the program wxAMPS. The simulation procedures of the effect of band offset between hole transport material (HTM) and perovskite layers were discussed.

2. Modeling of perovskite solar cell

Simulation methods describe the basic phenomena present in photovoltaic devices, allowing intuitive examination of each parameter and thus identifying the optimal operating conditions. In order to provide experimental direction, a theoretical study was performed using wxAMPS (Analysis of Microelectronic and Photonic Structure). The wxAMPS program assimilates intra-band tunneling model and trap-assisted tunneling model for more realistic aspects of heterojunction solar cells. The structure and energy band diagram of the employed device here are depicted in Figs. 1(a) and 1(b). In order to verify the effectiveness of our modelling approach, a device with NiO as HTM layer was first simulated and compared with reported experimental results. The AM 1.5G solar radiation spectrum was adopted as the illuminating source in the simulation. The light reflection of the top and the bottom contacts were set to be 0 and 1, respectively. The material parameters were summarized in Appendix A (Table A1) which was selected from reported experimental work.[51–59] Capture cross sections of both electrons and holes were set 1×10^{-16} cm^2 which result in a carrier diffusion length of ~ 1 μm in absorber materials. The thickness of the active layer was set 0.4 μm to arrange efficient carrier collection. The energy level defects in the simulated thin film materials were located at the middle of their band gap with the Gaussian type energetic distribution (characteristic energy of 0.1 eV). Tails characteristic energy was 0.01 eV with band tail density of states 1×10^{14} cm^{-3}/eV. The bimolecular electron-hole recombination rate has the most significant influence on the performance of the solar cell. Therefore two considerations were taken to set bimolecular recombination rate. In the first assumption, the conduction band electrons were directed to vacant states in the valence band. This process was labeled as band-to-band or direct recombination R_D (also known as intrinsic recombination). In the second assumption, electrons and holes recombine through intermediate gap states known as recombination centers. This was labeled as indirect recombination R_I (also known as extrinsic recombination) or Shockley, Read, and Hall recombination. The net recombination term $R(x)$ in the continuity equations takes both of these processes into consideration such that

$$R(x) = R_D(x) + R_I(x). \tag{1}$$

The bimolecular recombination rate simply relies on an overlap of electron and hole wavefunctions while Auger processes involve energy and momentum transfer of the recombining electron–hole pair to a third charge carrier. The experimental values of THz photoconductivity transients for perovskite materials have been reported[60] to get charge recombination rates associated with both bimolecular and monomolecular recombination rates as

$$\frac{dn}{dt} = -\gamma np - \gamma np_0, \tag{2}$$

where n is the photoinduced charge carrier density. The first term on the RHS of Eq. (2) represents bimolecular recombination rate between photogenerated carriers while the second term denotes mono-molecular recombination rate. In addition, the recombination dynamics of the free charge carrier density (n) could be described by the following differential equation:.[61]

$$\frac{dn}{dt} = -k_3n^3 - k_2n^2 - k_1n, \tag{3}$$

where k_3 is the decay constant describing Auger recombination, k_2 the bimolecular recombination constant, and k_1 the rate for monomolecular processes such as trap-assisted charge recombination. According to these equations the bimolecular recombination rate value was set to be 1×10^{-11} cm^3/s.[62] The surface recombination velocities of electrons and holes at the top and bottom electrodes were set to be 1×10^7 cm/s. The interface recombination velocity (S) was evaluated by a numerical approach

$$S_m = \frac{\int_{\text{int}} R\,dx}{m}, \tag{4}$$

where R is the recombination rate within the interface layer, int stands for the whole interface layer, and m denotes the concentration of holes and electrons. The exact values of R and m are obtained from the numerical solution, and the integral of R across the whole interface layer represents the total interface recombination as mentioned in Eq. (1).

It has been noticed that wxAMPS software does not take into account the interface recombination losses. To overcome this shortcoming, two thin defect layers were inserted artificially at the interfaces of HTL/absorber layer and

ETL/absorber layer as listed in supplementary information (Table A2). This allows to evaluate the role of interface modification in determining the performance of the device compatibility between simulated and experimental results.[59,63–67]

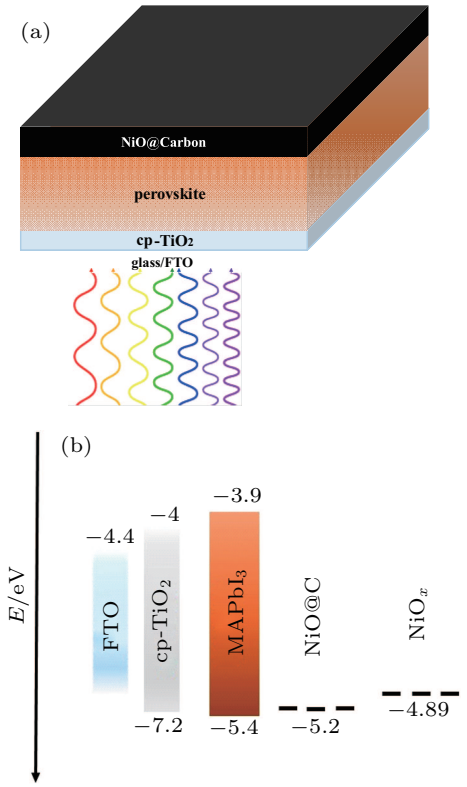


Fig. 1. (color online) (a) Schematic cross section of n–i–p perovskite solar cells. (b) Energy band diagram.

3. Results and discussion

The photocurrent density-voltage characteristics of the simulated devices with inorganic HTMs are shown in Fig. 2. An efficiency of 15% was obtained for the FTO/TiO_2/$MAPbI_3$/NiO_x/Au solar cell, closely reproducing the results reported by Liu *et al.*[43] The simulated current density is higher than the reported experimental data, which may be ascribed to the neglect of interface losses and the deposition constraint of non-stoichiometric NiO_x in regular device configuration. Replacing NiO_x with a new high mobility hole transporting material such as NiO@Carbon to get highly efficient regular planar heterojunction PSCs at low cost could be a promising route to fabrication via screen printing, doctor blading, and spin coating.[68] Further, the simulated investigations were focused on the effect of electrical conductivity of NiO@Carbon to provide a theoretical guideline in the performance of PSCs. Significantly, enhanced electrical conductivity, high fill factor (FF), and increased short circuit current density (J_{sc}) are observed in the NiO@carbon based PSCs as depicted in Fig. 2.

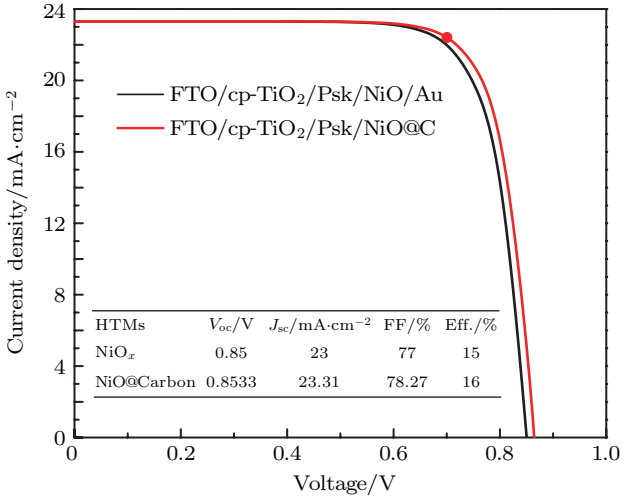


Fig. 2. (color online) Simulated photovoltaic characteristics, Psk = perovskite, cp = compact. Inset shows the photovoltaic parameters of the corresponding devices.

A further investigation on photoelectric behaviors of the device is shown in Fig. 3, whereby the recombination rate is illustrated to decrease with the efficient hole extraction through NiO@carbon-HTM. In fact, a pretty low trap-assisted recombination rate is observed in $MAPbI_3$ films. This is closely related to the experimental values using transient THz spectroscopy.[69] The reduced recombination rate further corresponds to high V_{oc}, which is comparable with the one measured from transient V_{oc} decay experiment and intensity-modulated photovoltage spectroscopy (IMVS) method.[70] The performances of the proposed device are also attributed to low series resistance, efficient hole transport, and avoiding the possible formation of the Schottky junction at the HTM/CE interface.[41,42,46]

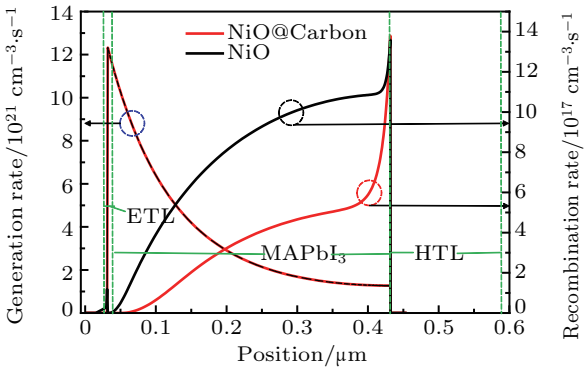


Fig. 3. (color online) Trends of carrier recombination and generation rates in PSCs based on NiO@Carbon and NiO hole transport materials.

Additionally, the impact of the band offset between HTMs/active layers on the performance of the device was also investigated. A thin absorber layer with higher defect density was inserted between HTM layer and the active layer to take into account interfacial carrier recombination. The discontinuous energy band diagram is due to the different electron affinity of the materials involved in the heterojunction. Figure 1(b)

depicts the energy-level-alignment diagram of the PSC components before equilibrium (relative to the vacuum level) and the dashed lines depict the Fermi levels of different layers. Inorganic metal oxides possess advantages such as energetically favorable energy level alignment with perovskite layer with a deep-lying valence band. Therefore, the valance band offset between HTM/active layers is a key factor for carrier recombination at the interfaces, and thus determining open-circuit voltage (V_{oc}) to some extent through Fermi level pinning effect.

Indeed, the efficient device was obtained through optimization of the band offset matching of the materials at the interface to allow efficient holes extraction from the perovskite to valence band maximum (VBM) of the HTM without obvious energy loss. In this regard, we use the definition of electron affinity as follows:

$$\Delta E_c = \Delta\chi, \tag{5}$$

$$\Delta E_v = \Delta E_g - \Delta\chi, \tag{6}$$

where $\Delta\chi$ is the difference of the electron affinity, ΔE_g is the difference of the band gapes, ΔE_c the conduction band offset, and ΔE_v the valence band offset.

The influence of ΔE_v on the performance of the solar cells was explored while maintaining the constant value of ΔE_g. The effect of ΔE_c between HTM and perovskite was not included in this study because the electron is significantly small, thus the carrier recombination associated with band offset should be negligible. The hole tunneling mechanism was simulated via wxAMPS when there is a barrier caused by band offset. The results reveal a quantitative basis for choosing an optimal hole extraction layer. The hole layer exhibits the value of VBM of -5.28 eV ($\Delta E_v = -0.15$ eV) to -5.78 eV ($\Delta E_v = -0.35$ eV) with the energy band of the perovskite solar cell using NiO as HTM as shown in Fig. 4.

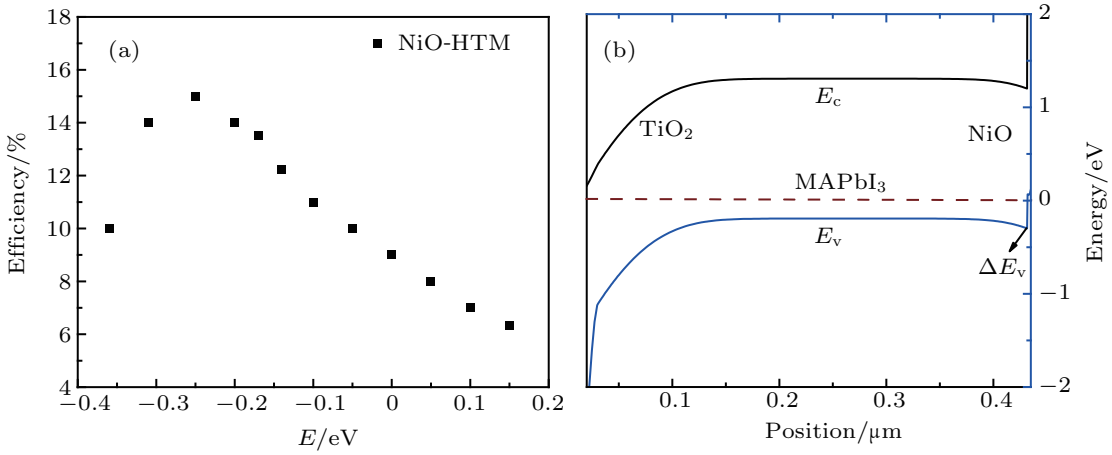


Fig. 4. (color online) (a) Effect of ΔE_v on the efficiency of the perovskite solar cell. (b) Energy band of the perovskite solar cell using nickel oxide as HTM.

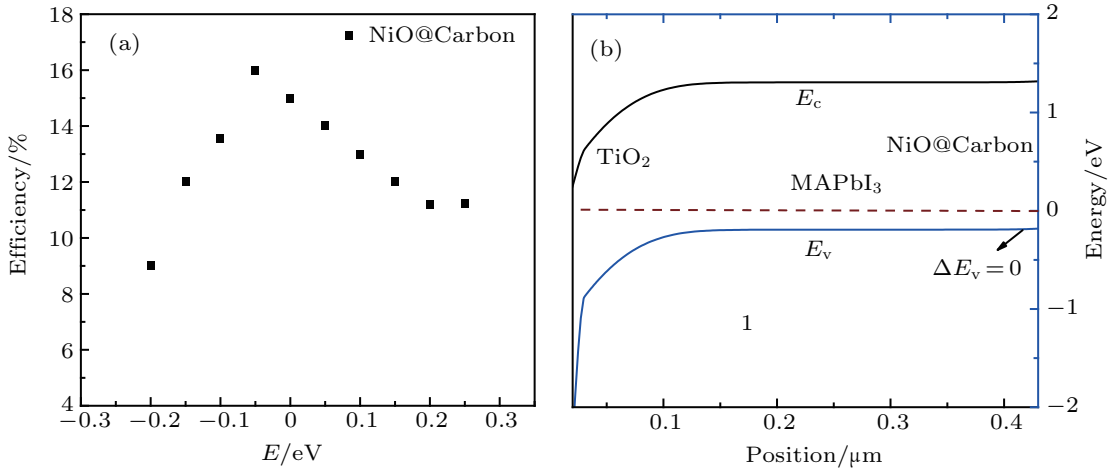


Fig. 5. (color online) (a) Effect of ΔE_v on the efficiency of the perovskite solar cell. (b) Energy band of the perovskite solar cell using NiO@carbon as HTM.

When the VBM of the HTM was slightly lower than the VBM of the perovskite ($\Delta E_v < 0$), a hole extraction barrier cliff was formed at the interface of HTM/absorber layer. Although the V_{oc} increases by further separation of the valence band in the reverse direction, the barrier takes the dominant role in decreasing the FF. This was related to large difference between the VBM of the HTM and perovskite. On the other hand, when ΔE_v was positive, the VBM of HTM was above the perovskite VBM which restricted the built-in voltage and resulted in lower efficiency. Thus, the optimum position of the valence band of HTM was derived to be -0.1 to -0.3 eV lower than that of the perovskite layer. In addition, figures 5(a) and 5(b) reveal the impact of band offset on the performance of the PSC and energy band position using NiO@carbon as HTM. When the ΔE_v is positive, V_{oc} decreases with increasing ΔE_v. However, V_{oc} is increased due to the decreasing ΔE_v which is more prominent when the VBM of HTM matches with the perovskite VBM. In conclusion, the optimum ΔE_v between the perovskite and HTM based on NiO@Carbon is derived to be -0.15 to 0.15 eV.

4. Conclusion

NiO@carbon was simulated using wxAMPS software as an update of the popular solar cell simulation tool (AMPS; analysis of microelectronic and photonic structures). The models of solar cells were constructed with thin film stacks of glass/FTO/cp-TiO_2/$MAPbI_3$/NiO@carbon. The shortcoming in each device configuration was write minimized instead of performed by inserting thin defect layers at the interfaces of HTL/absorber layer and ETL/absorber layer. Simulation results indicate that owing to the low ΔE_v, combined with superior conductivity, NiO@carbon HTM can exhibit both high V_{oc} and J_{sc} values. Additionally, low recombination rates, efficient hole transport, and avoiding the possible formation of the Schottky junction at the HTM/CE interface led to an inspiring efficiency of 16% under moderate conditions, further highlighting the great potential of NiO@carbon HTM in achieving high PCEs. In particular, such inorganic HTM could be fabricated through doctor blading and screen printing techniques for the device optimization at low cost. The results simulated here should provide both the insight and understanding of the role of NiO@Carbon HTM in PSCs and help to establish device parameters that allow for further analysis and design optimization.

Appendix A

Table A1. Basic parameters of the materials.

Parameters and units	TiO_2 (ETL)	$MAPbI_3$	NiO (HTL)	NiO@Carbon
Dielectric constant	100	30	11	12
Band gap/eV	3.2	1.5	3.6	3.31
Electron affinity/eV	4	3.93	1.46	2
Thickness/nm	30	400	50	100
Electron and hole mobility/$cm^2 \cdot V^{-1} \cdot s^{-1}$	0.006, 0.006	50,50	0.5	0.6
Acceptor concentration/cm^{-3}	0	2.14×10^{17}	1.5×10^{18}	2.4×10^{21}
Donor concentration/cm^{-3}	5×10^{19}	0	0	0
Effective conduction band density/cm^{-3}	1×10^{21}	2.5×10^{20}	1.6×10^{19}	1.4×10^{22}
Effective valence band density/cm^{-3}	2×10^{20}	2.5×10^{20}	1.1×10^{19}	1.5×10^{20}
Characteristic energy for donor and acceptor like tails/eV	0.01, 0.01	0.015, 0.015	0.01, 0.01	0.01, 0.01
Band tail density of states/$cm^{-3} \cdot eV^{-1}$	1×10^{14}	1×10^{14}	1×10^{14}	1×10^{14}
Capture cross section for electrons and holes in donor tail states/cm^2	1×10^{-15}, 1×10^{-17}	1×10^{-15}, 1×10^{-17}	1×10^{-15}, 1×10^{-17}	1×10^{-15}, 1×10^{-17}
Capture cross section for electrons and holes in acceptor tail states/cm^2	1×10^{-17}, 1×10^{-15}	1×10^{-17}, 1×10^{-15}	1×10^{-17}, 1×10^{-15}	1×10^{-17}, 1×10^{-15}
Gaussian defects donor and acceptor states density/cm^{-3}	1×10^{18}, 1×10^{18}	1×10^{17}, 1×10^{17}	1×10^{18}, 1×10^{18}	1×10^{18}, 1×10^{18}
Gaussian defects donor and acceptor peak energy/eV	1.1, 1.1	1.2, 1.2	1.1, 1.1	1.1, 1.1
Standard deviation/eV	0.1, 0.1	0.1, 0.1	0.1, 0.1	0.1, 0.1
Capture cross section of donor-like Gaussian state for electrons and holes/cm^2	1×10^{-19}, 1×10^{-18}	1×10^{-20}, 1×10^{-19}	1×10^{-19}, 1×10^{-18}	1×10^{-19}, 1×10^{-18}
Capture cross section of acceptor-like Gaussian state for electrons and holes/cm^2	1×10^{-18}, 1×10^{-19}	1×10^{-19}, 1×10^{-20}	1×10^{-18}, 1×10^{-19}	1×10^{-18}, 1×10^{-19}

Table A2. Basic parameters for thin films defect layers at the interfaces of ETM/perovskite and HTM/perovskite.

Parameters and units	ETM/perovskite	HTM/perovskite
Dielectric constant	30	11
Band gap/eV	1.5	3.6
Electron affinity/eV	3.93	1.46
Thickness/nm	2	2
Electron and hole mobility/$cm^2 \cdot V^{-1} \cdot s^{-1}$	50,50	0.5, 0.5
Acceptor concentration/cm^{-3}	2.14×10^{17}	1.4×10^{20}
Donor concentration/cm^{-3}	0	0
Effective conduction and density/cm^{-3}	2.5×10^{20}	2×10^{17}
Effective valence band density/cm^{-3}	2.5×10^{20}	1.1×10^{19}
Characteristic energy for donor and acceptor-like tails /eV	0.015, 0.015	0.01, 0.01
Band tail density of states/$cm^{-3} \cdot eV^{-1}$	1×10^{14}	1×10^{14}
Capture cross section for electrons and holes in donor tail states/cm^2	1×10^{-15}, 1×10^{-17}	1×10^{-15}, 1×10^{-17}
Capture cross section for electrons and holes in acceptor tail states/cm^2	1×10^{-17}, 1×10^{-15}	1×10^{-17}, 1×10^{-15}
Switch-over energy/eV	0.7	0.8
Density of mid-gap acceptor and donor-like states/$cm^{-3} \cdot eV^{-1}$	1×10^{16} to 1×10^{19}	1×10^{17} to 1×10^{19}
Capture cross section of electrons and holes in donor mid-gap states/cm^2	1×10^{-17}, 1×10^{-18}	1×10^{-16}, 1×10^{-17}
Capture cross section of electrons and holes in acceptor mid-gap states/cm^2	1×10^{-18}, 1×10^{-17}	1×10^{-17}, 1×10^{-16}

References

[1] Kojima A, Teshima K, Shirai Y and Miyasaka T 2009 *J. Am. Chem. Soc.* **131** 6050

[2] Lee M M, Teuscher J, Miyasaka T, Murakami T N and Snaith H J 2012 *Science* **338** 643

[3] Kim H S, Lee C R, Im J H, Lee K B, Moehl T, Marchioro A, Moon S J, Humphry-Baker R, Yum J H and Moser J E 2012 *Sci. Rep.* **2**

[4] Burschka J, Pellet N, Moon S J, Humphry-Baker R, Gao P, Nazeeruddin M K and Grätzel M 2013 *Nature* **499** 316

[5] Liu M, Johnston M B and Snaith H J 2013 *Nature* **501** 395

[6] Jeon N J, Noh J H, Kim Y C, Yang W S, Ryu S and Seok S I 2014 *Nat. Mater.* **13** 897

[7] Jeon N J, Noh J H, Yang W S, Kim Y C, Ryu S, Seo J and Seok S I 2015 *Nature* **517** 476

[8] Yang W S, Noh J H, Jeon N J, Kim Y C, Ryu S, Seo J and Seok S I 2015 *Science* **348** 1234

[9] Yuan X Z, Chao W and Shi H 2017 *Chin. Phys. Lett.* **34** 047304

[10] Yao J, Wei Q, Ma Q Y and Wu D J 2017 *Chin. Phys. B* **26** 057302

[11] Zeng H D, Zhu Z Y, Zhang J D and Cheng X L 2017 *Chin. Phys. B* **26** 056101

[12] Liu P, Yang B C, Liu G, Wu R S, Zhang C J, Wang F, Li S G, Yang J L, Gao Y L and Zhou C H 2017 *Chin. Phys. B* **26** 058401

[13] Rashad M M, Elseman A M and Hassan A M 2016 *Optik-International Journal for Light and Electron Optics* **127** 9775

[14] Yan W, Ye S, Li Y, Sun W, Rao H, Liu Z, Bian Z and Huang C 2016 *Adv. Energy Mater.* **6** 17

[15] Li M H, Shen P S, Wang K C, Guo T F and Chen P 2015 *J. Mater. Chem. A* **3** 9011

[16] Yang L Cai F Yan Y Li J Liu D Pearson A J and Wang T 2017 *Adv. Function. Mater.*

[17] Zhao D, Sexton M, Park H Y, Baure G, Nino J C and So F 2015 *Adv. Energy Mater.* **5** 6

[18] Zuo C and Ding L 2015 *Small* **11** 5528

[19] Elseman A M, Rashad M M and Hassan A M 2016 *ACS Sustainable Chemistry & Engineering* **4** 4875

[20] Zhang J, Gu P, Xu J, Xue H and Pang H 2016 *Nanoscale* **8** 18578

[21] Chen W, Xu L, Feng X, Jie J and He Z 2017 *Adv. Mater.* **29** 16

[22] Rao H, Ye S, Sun W, Yan W, Li Y, Peng H, Liu Z, Bian Z, Li Y and Huang C 2016 *Nano Energy* **27** 51

[23] Trifiletti V, Roiati V, Colella S, Giannuzzi R, De Marco L, Rizzo A, Manca M, Listorti A and Gigli G 2015 *ACS Applied Materials & Interfaces* **7** 4283

[24] Cao K, Zuo Z, Cui J, Shen Y, Moehl T, Zakeeruddin S M, Grätzel M and Wang M 2015 *Nano Energy* **17** 171

[25] Park J H, Seo J, Park S, Shin S S, Kim Y C, Jeon N J, Shin H W, Ahn T K, Noh J H and Yoon S C 2015 *Adv. Mater.* **27** 4013

[26] Cui J, Meng F, Zhang H, Cao K, Yuan H, Cheng Y, Huang F and Wang M 2014 *ACS Appl. Mater. Interf.* **6** 22862

[27] Wang K C, Shen P S, Li M H, Chen S, Lin M W, Chen P and Guo T F 2014 *ACS Appl. Mater. Interf.* **6** 11851

[28] Liu Z, Zhang M, Xu X, Cai F, Yuan H, Bu L, Li W, Zhu A, Zhao Z and Wang M 2015 *J. Mater. Chem. A* **3** 24121

[29] Yin X, Liu J, Ma J, Zhang C, Chen P, Que M, Yang Y, Que W, Niu C and Shao J 2016 *J. Power Sources* **329** 398

[30] Cui J, Li P, Chen Z, Cao K, Li D, Han J, Shen Y, Peng M, Fu Y Q and Wang M 2016 *Appl. Phys. Lett.* **109** 171103

[31] Kwon U, Kim B G, Nguyen D C, Park J H, Ha N Y, Kim S J, Ko S H, Lee S, Lee D and Park H J 2016 *Sci. Rep.* **6** 30759

[32] Subbiah A S, Halder A, Ghosh S, Mahuli N, Hodes G and Sarkar S K 2014 *J. Phys. Chem. Lett.* **5** 1748

[33] Jeng J Y, Chen K C, Chiang T Y, Lin P Y, Tsai T D, Chang Y C, Guo T F, Chen P, Wen T C and Hsu Y J 2014 *Adv. Mater.* **26** 4107

[34] Hu L, Peng J, Wang W, Xia Z, Yuan J, Lu J, Huang X, Ma W, Song H and Chen W 2014 *Acs Photon.* **1** 547

[35] Hou Y, Chen W, Baran D, Stubhan T, Luechinger N A, Hartmeier B, Richter M, Min J, Chen S and Quiroz C O R 2016 *Adv. Mater.* **28** 5112

[36] Yin X, Chen P, Que M, Xing Y, Que W, Niu C and Shao J 2016 *ACS Nano* **10** 3630

[37] You J, Meng L, Song T B, Guo T F, Chang W H, Hong Z, Chen H, Zhou H, Chen Q and Liu Y 2016 *Nat. Nanotech.* **11** 75

[38] Seo S, Park I J, Kim M, Lee S, Bae C, Jung H S, Park N G, Kim J Y and Shin H 2016 *Nanoscale* **8** 11403

[39] Corani A, Li M H, Shen P S, Chen P, Guo T F, El Nahhas A, Zheng K, Yartsev A, Sundström V and Ponseca Jr C S 2016 *J. Phys. Chem. Lett.* **7** 1096

[40] Chen W, Zhu Y, Yu Y, Xu L, Zhang G and He Z 2016 *Chem. Mater.* **28** 4879

[41] Chen W, Wu Y, Yue Y, Liu J, Zhang W, Yang X, Chen H, Bi E, Ashraful I and Grätzel M 2015 *Science* **350** 944

[42] Chen W, Liu F Z, Feng X Y, Djurišić A B, Chan W K and He Z B 2017 *Adv. Energy Mater.*

[43] Liu Z, Zhu A, Cai F, Tao L, Zhou Y, Zhao Z, Chen Q, Cheng Y B and Zhou H 2017 *J. Mater. Chem. A* **5** 6597

[44] Lany S, Osorio-Guillén J and Zunger A 2007 *Phys. Rev. B* **75** 241203

[45] Zhang K H, Xi K, Blamire M G and Egdell R G 2016 *J. Phys.: Conden. Matter* **28** 383002

[46] Jung J W, Chueh C C and Jen A K Y 2015 *Adv. Mater.* **27** 7874

[47] Yang Z, Chueh C C, Liang P W, Crump M, Lin F, Zhu Z and Jen A K Y 2016 *Nano Energy* **22** 328

[48] Rajagopal A, Williams S T, Chueh C C and Jen A K Y 2016 *J. Phys. Chem. Lett.* **7** 995
[49] Natu G, Hasin P, Huang Z, Ji Z, He M and Wu Y 2012 *ACS Appl. Mater. Interf.* **4** 5922
[50] Liu M H, Zhou Z J, Zhang P P, Tian Q W, Zhou W H, Kou D X and Wu S X 2016 *Opt. Express* **24** A1349
[51] Elseman A, Shalan A, Rashad M and Hassan A 2017 *Mater. Sci. Semicond. Process.* **66** 176
[52] Son M K, Steier L, Schreier M, Mayer M T, Luo J and Grätzel M 2017 *Energy & Environmental Science* **10** 912
[53] Sato K, Kim S, Komuro S and Zhao X 2016 *Jpn J. Appl. Phys.* **55** 06GJ10
[54] Vahini R, Kumar P S and Karuthapandian S 2016 *Appl. Phys. A* **122** 1
[55] Wang M, Han J, Hu Y, Guo R and Yin Y 2016 *ACS Appl. Mater. Interf.* **8** 29511
[56] Yang X, Wu G, Zhu C, Zou W, Gao Y, Tian J and Zheng Z 2016 *J. Colloid Interface Science* **469** 287
[57] Akhtar N, El-Safty S A, Abdelsalam M E and Kawarada H 2015 *Adv. Healthcare Mater.* **4** 2110
[58] Litzov I and Brabec C J 2013 *Materials* **6** 5796
[59] Liu F, Zhu J, Wei J, Li Y, Lv M, Yang S, Zhang B, Yao J and Dai S 2014 *Appl. Phys. Lett.* **104** 253508
[60] Noel N K, Stranks S D, Abate A, Wehrenfennig C, Guarnera S, Haghighirad A A, Sadhanala A, Eperon G E, Pathak S K and Johnston M B 2014 *Energy & Environmental Science* **7** 3061
[61] Wehrenfennig C, Liu M, Snaith H J, Johnston M B and Herz L M 2014 *Energy & Environmental Science* **7** 2269
[62] Wang Y Xia Z Liu Y and Zhou H 2015 *Simulation of Perovskite Solar Cells with Inorganic Hole Transporting Materials*. In *Photovoltaic Specialist Conference (PVSC)*, 2015 IEEE 42nd, p. 1
[63] Cuiffi J, Benanti T, Nam W J and Fonash S 2010 *Appl. Phys. Lett.* **96** 73
[64] Kemp K W, Labelle A J, Thon S M, Ip A H, Kramer I J, Hoogland S and Sargent E H 2013 *Adv. Energy Mater.* **3** 917
[65] Wang T, Chen J, Wu G, Song D and Li M 2017 *Journal of Semiconductors* **38** 014005
[66] Wang T, Chen J, Wu G and Li M 2016 *Sci. China Mater.* **59** 703
[67] Boussettine A, Belhadji Y and Benmansour A 2012 *Energy Procedia* **18** 693
[68] Gao M W, Ye C, Wang X Y, He Y S, Guo J M and Yang P F 2016 *Chin. Phys. B* **25** 075202
[69] Wehrenfennig C, Eperon G E, Johnston M B, Snaith H J and Herz L M 2014 *Adv. Mater.* **26** 1584
[70] Bi D, Yang L, Boschloo G, Hagfeldt A and Johansson E M 2013 *J. Phys. Chem. Lett.* **4** 1532